Controlling Non-Franck−Condon Transitions: Counterintuitive Schemes of Population Transfer in the Adiabatic and Strong Adiabatic Regimes†

Vladimir S. Malinovsky

Michigan Center for Theoretical Physics & FOCUS Center, Department of Physics, University of Michigan, Ann Arbor, Michigan 48109

Jesuś Santamaría

Departamento de Química Física, Universidad Complutense, 28040 Madrid, Spain

Ignacio R. Solá*

Department of Chemistry, Princeton University, Princeton, New Jersey 08544, and Departamento de Química Física, Universidad Complutense, 28040 Madrid, Spain

Received: December 30, 2002; In Final Form: May 12, 2003

Vibrationally selective population transfer in electronic transitions involving small Franck−Condon factors is studied by means of two-photon excitation with pulse sequences applied in counterintutive order. Depending on the intensity of the pulses, two schemes allow ultrafast adiabatic passage. Both schemes, called STIRAP and APLIP, are analyzed as a function of the geometry of the electronic states and of the time duration and intensity of the pulses that drive the transitions. Although both schemes imply adiabatic following, the APLIP scheme requires pulses of considerably larger intensity than STIRAP, hence operating in a strong adiabatic regime. Simple adiabatic criteria for high-quality transfer are proposed, and analytic proofs are provided that show under which conditions STIRAP and APLIP converge. The results of this paper are illustrated with numerical simulations for two different electronic transitions in the Na_2 molecule.

I. Introduction

State selective preparation of molecules in excited states is often a fundamental step for subsequent study of unimolecular or bimolecular reactions, with applications in photochemistry, spectroscopy, and laser technology.[1] We consider electronic transitions that lead to no vibrational excitation in the bond coordinate. Since usually the equilibrium configurations are more relaxed in excited electronic states than in the ground state, the laser pulses must be tailored in specific ways in order to avoid the direct dipole-preferred Franck−Condon or vertical transition that leads to vibrational excitation. This is what we refer herein as controlling non-Franck−Condon transitions.

Several schemes and even general methodologies have been proposed to find the best pulses that drive the vibrational population to specific quantum states.[2,3] In this paper we study a class of schemes that involve robust population transfer by adiabatic passage.[4] In these schemes, one usually proceeds by designing frequency chirped pulses or different pulse sequences so that the initial ($\phi_i(x)$) and the target ($\phi_f(x)$) states are connected via a single eigenstate of the Hamiltonian in the adiabatic representation, which is called the transfer state.[4]

We consider one general solution on the basis of two pulses that act on the system in counterintuitive order.[5−7] That is, the pulse that drives the transition between a selected intermediate state, $\phi_b(x)$, and the target state $\phi_f(x)$, precedes the pulse that drives the transition between $\phi_i(x)$ and $\phi_b(x)$. The method, initially proposed for population transfer by stimulated Raman adiabatic passage (STIRAP) in 3-level systems,[5,6] has been experimentally applied to atomic and Raman transitions using continuous wave (CW) lasers and nanosecond pulses.[7] Here we address the problems involved with its implementation for selective non-Franck−Condon electronic transitions in the Na_2 molecule with pico- or subpicosecond laser pulses. We analyze the properties of the population transfer as a function of the geometrical features of the electronic potentials, as well as the time duration and intensity of the pulses that drive the excitation.

There are other possible ways to address the problem of selective population transfer in electronic transitions. A very general methodology uses optimal control[8,9] or learning algorithms[10] to find the optimal pulses that drive the dynamics to the desired target state. One difficulty with the methodology of optimal control is related with the physical interpretation of the mechanisms underlying the dynamics, which are often obscure. Also, the optimal dynamics are usually very sensitive with respect to the final time chosen to maximize the yield of the desired selective transition, making the results more difficult to interpret and generalize when considering the properties of the population transfer as a function of the geometry of the system and the time duration and intensity of the pulses. Although there are prospects for devising feasible schemes to obtain mechanistic information easily applicable to optimal control design,[11] for the type of analysis explored in this paper, the approach based on schemes designed a priori as the counterintuitive pulse sequence here proposed is usually simpler. The dynamical features of the process are now anticipated on the basis of the properties of analytical or quasi-analytical

† Part of the special issue "A. C. Albrecht Memorial Issue".

* To whom correspondence should be addressed. E-mail: ignacio@wfn-shop.princeton.edu.

10.1021/jp0226477 CCC: $25.00
Published on Web 07/23/2003

models, which are proposed for the dynamics of simple quantum systems.[12] In this case, the approach is valuable when the molecular Hamiltonian of the system of interest accepts the simplifying assumptions of the chosen model, that is, when a reduced dimensional description of the Hamiltonian provides trustful results.[2] Therefore, a major concern is the implementation of the model on a realistic scenario.

A general advantage of adiabatic methods over other coherent excitations is that the adiabatic schemes assess greater stability on the dynamics relying in the control of very few parameters with ample margins. However, this economy in the variables to control is at the expense of energy in the field, since a typical condition for adiabatic following requires the effective pulse area to be much larger than π [7]

$$\Omega_{\text{eff}}\tau \gg \pi \tag{1}$$

(which can sometimes be as much as 100), where Ω_{eff} is the effective Rabi frequency or radiation coupling term of the process and τ is the time scale or width of the pulses. This is to be compared with a minimum of $\Omega_{\text{eff}}\tau = \pi$ required for population inversion according to the Rabi formula, which underlies many other possible coherent excitation schemes.

In two-photon electronic transitions, the effective Rabi frequency depends on the amplitude of the laser times the Franck−Condon amplitudes between the chosen intermediate quantum state $\phi_b(x)$ and both $\phi_i(x)$ and $\phi_f(x)$. In STIRAP, the wave function $\phi_b(x)$, which we call the wave function bridge, must be orthogonal to the adiabatic transfer state. The adiabatic passage relies on a fine engineering of the Hamiltonian in the adiabatic representation, which usually requires isolating $\phi_b(x)$ from all other vibrational levels. For some non-Franck−Condon electronic transitions it is not always possible to find a proper intermediate state that satisfies these requirements using ultrashort laser pulses. For instance, following eq 1, for small τ, adiabatic following requires large Ω_{eff}. For small Franck−Condon factors the laser amplitudes must be very large, inducing other preferred vibronic transitions and breaking the validity of the 3-level Hamiltonian description required for STIRAP. In the STIRAP frame, the adiabaticity and selectivity cannot be restored by further increasing the amplitudes of the pulses. As a consequence of the time−energy uncertainty principle, in this regime a wave packet can be formed and subsequently evolve, much in the same way as (or actually complementary to) the way the time uncertainty of femtosecond pulses can be hold responsible for inducing the dynamics in ultrafast processes. Therefore, a completely new model must be used to first understand and then control the dynamics in these conditions.

Several interesting phenomena have been predicted and observed by using strong ultrafast laser pulses.[13] The underlying model to understand processes such as bond softening[14] and stabilization[15] is based on the structure of the electronic potentials in the adiabatic representation, so-called light-induced potentials (LIPs).[13] Recently, counterintuitive pulse sequences have been proposed to shape dynamically the structure of the LIPs so as to allow the population transfer of the vibrational wave function between different electronic states.[16] Adiabatic passage by light-induced potentials (APLIP) has been studied and generalized for different scenarios and purposes.[16−22] In comparison with STIRAP, the APLIP scheme can be thought of as an adiabatic scheme that requires only crude engineering of the Hamiltonian. Increasing the pulses amplitude introduces more energy in the system, so that the intermediate electronic potential can be considered as a pool of wave function bridges that the system uses to go from $\phi_i(x)$ to $\phi_f(x)$. In this situation the analysis of the adiabatic requirements needs further elucidation, since eq 1 no longer sets sufficient conditions for selective population transfer.

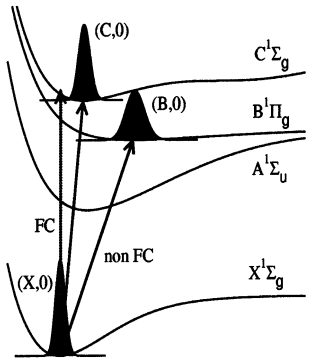

Figure 1. Na_2 potentials considered for population transfer from the initial to two possible target wave functions, defining the so-called XAB and XAC systems. Depending on the final state, the proposed transition implies a larger or smaller displacement of vibrational population along the bond coordinate, so that the overall two-photon transition can be almost Franck−Condon type (XAC) or highly non-Franck−Condon type (XAB).

In this paper we are primarily concerned with analyzing properties of the population transfer in APLIP on the basis of the simplest Hamiltonian model, as a function of the geometry, time duration, and intensity of the pulses, and comparing these properties with those of the STIRAP method. The organization of this paper is the following. In section 2 we introduce the molecular model of the Na_2 molecule and the numerical methods employed to solve the dynamics in that system. In particular we propose the optimization of two selective non-Franck−Condon electronic transitions to different final electronic states. In section 3 we consider an implementation of STIRAP in Na_2 in view of the basic properties of the STIRAP Hamiltonian and we study the subsequent dynamics of the system. In section 4 we show how the population transfer depends on the amplitude and duration of the pulses. In particular it is shown where the different regimes of STIRAP and APLIP work. In section 5 we study the dynamics via APLIP and we analyze the role of geometry, intensity, and duration of the field and show when the STIRAP and APLIP dynamics converge. In section 6 are the final remarks.

II. Molecular Model and Numerical Procedure

We choose the Na_2 dimer as our molecular candidate to test the previous adiabatic schemes, since the electronic curves of many excited states are well-known and the energetics of the system is well suited for experimental implementation. In fact, Na_2 was the first molecule where STIRAP was demonstrated.[6]

In Figure 1 we show the electronic curves that participate in the model. Our initial state is the zeroth vibrational level in the ground electronic state, that we call (X,0), with wave function $\phi_0^X(x)$. The goal is to invert the population to the zeroth vibrational level of either the excited electronic state B $^1\Pi_g$, which we name as $\phi_0^B(x)$ or (B,0), or the excited electronic state C $^1\Sigma_g$, which we name $\phi_0^C(x)$ or (C,0).

In both excited configurations the bond is more relaxed than in the ground state, and therefore, the transitions that we are considering are highly non-Franck−Condon (see Figure 1). However, while $\phi_0^X(x)$ still overlaps with $\phi_0^C(x)$, its overlap with $\phi_0^B(x)$ is negligible. The results of population transfer depending on the target state selected show the different sensitivity of STIRAP and APLIP with respect to the geometry of the excited states.

The numerical results of the paper are obtained by solving the Schrödinger equation driven by two control fields, $\epsilon_1(t)$ and $\epsilon_2(t)$, in the rotating wave approximation (RWA) and in the coordinate representation, including only 3 potential curves for each calculation (the ground, the intermediate electronic potential A $^1\Sigma_u$, and the chosen final electronic state):

$$i\hbar\frac{\partial}{\partial t}\begin{pmatrix}\psi_1(x,t)\\ \psi_2(x,t)\\ \psi_3(x,t)\end{pmatrix} = \left[-\frac{\hbar^2}{2m}\frac{\partial^2}{\partial x^2}\mathscr{I} + \begin{pmatrix}U_1(x) & -\hbar\Omega_1(t)/2 & 0\\ -\hbar\Omega_1(t)/2 & U_2(x) & -\hbar\Omega_2(t)/2\\ 0 & -\hbar\Omega_2(t)/2 & U_3(x)\end{pmatrix}\right]\begin{pmatrix}\psi_1(x,t)\\ \psi_2(x,t)\\ \psi_3(x,t)\end{pmatrix} \quad (2)$$

Here $\mathscr{I}$ is the unity matrix and $U_i(x)$ are the energy shifted potentials: $U_1(x) = V_X(x)$, $U_2(x) = V_A(x) - \hbar\omega_1$, $U_3(x) = V_B(x) - \hbar(\omega_1 + \omega_2)$ or $U_3(x) = V_C(x) - \hbar(\omega_1 + \omega_2)$, with ω_1 and ω_2 the laser carrier frequencies. To simplify the analysis regarding how the geometry of the potentials affects the results, we assume the Franck−Condon approximation and, without loss of generality, write $\mu_{12}(x) = \mu_{23}(x) = 1$. In the coordinate representation the Rabi frequencies are then exactly the laser amplitudes in frequency units, $\Omega_1(t) = \epsilon_1(t)/\hbar$ and $\Omega_2(t) = \epsilon_2(t)/\hbar$, where, following the RWA, the pulses are represented only by the envelope function. We choose Gaussian-shaped pulses for all the results presented in the paper, $\epsilon_1(t) = \epsilon_1^0 \exp(-(t \pm \tau)^2/2\sigma^2)$ and $\epsilon_2(t) = \epsilon_{10} \exp(-(t \mp \tau)^2/2\sigma^2)$, where 2τ is the time delay between the pulses. Equation 2 is solved by a standard split-operator propagator combined with fast Fourier transform techniques. More details can be found in ref 23.

III. Stirap in Molecular Systems

A. Population Inversion in Molecular Systems via STIRAP. The STIRAP scheme is a method of adiabatic passage that controls the population transfer via an intermediate level by applying a counterintuitive pulse sequence, such that the laser that couples the intermediate ($\phi_b(x)$) with the target state ($\phi_f(x)$), $\epsilon_2(t)$, *precedes* the laser that couples the initial state ($\phi_i(x)$) with $\phi_b(x)$, $\epsilon_1(t)$. To implement the STIRAP scheme in any realistic system, one needs to find a good intermediate state, such that its wave function works as an effective bridge between the initial and final states. The efficiency of the method relies on the validity of the model, whose general Hamiltonian, implying the rotating wave approximation (RWA) and using resonant pulses, is formulated as[7]

$$\mathscr{H}_{STIRAP} = \frac{\hbar}{2}\begin{pmatrix}0 & -\Omega_1(t) & 0\\ -\Omega_1(t) & 0 & -\Omega_2(t)\\ 0 & -\Omega_2(t) & 0\end{pmatrix} \quad (3)$$

The coupling elements are defined in terms of the Rabi frequencies, $\Omega_1(t) = \epsilon_1(t)\mu_{ib}/\hbar$ and $\Omega_2(t) = \epsilon_2(t)\mu_{bf}/\hbar$, where μ_{ib} and μ_{bf} are the dipole moments between the "bridge" state and the initial and final states, respectively.

The physical mechanism of STIRAP is easily explained by following the dynamics in the adiabatic representation, which is obtained by diagonalizing the Hamiltonian via the rotation matrix

$$\mathscr{R}_S(t) = \frac{1}{\sqrt{2}}\begin{pmatrix}\sin\theta & \sqrt{2}\cos\theta & \sin\theta\\ 1 & 0 & -1\\ \cos\theta & -\sqrt{2}\sin\theta & \cos\theta\end{pmatrix} \quad (4)$$

where $\theta(t) = \arctan(\Omega_1(t)/\Omega_2(t))$ is the adiabatic mixing angle. The transfer state responsible for the adiabatic passage is the dressed state (eigenstate of the adiabatic Hamiltonian) of zero eigenvalue:

$$\Phi_0(x,t) = \frac{1}{\Omega_0(t)}(\Omega_2(t)\phi_i(x) - \Omega_1(t)\phi_f(x)) \quad (5)$$

Here $\Omega_0(t) = \sqrt{\Omega_1(t)^2 + \Omega_2(t)^2}$ serves as a normalization factor. By the choice of a counterintuitive pulse sequence (such that $\Omega_2(t) \gg \Omega_1(t)$ at initial times and $\Omega_2(t) \ll \Omega_1(t)$ at late times), $\Phi_0(x,t)$ correlates with $\phi_i(x)$ at initial times and with $\phi_f(x)$ at late times and, therefore, as long as the dynamic evolution is adiabatic, serves its purpose as a transfer state. In its simpler form, the adiabaticity can be assessed[7] if

$$\Omega_0\sigma \gg 1 \quad (6)$$

where σ is the time delay or the time width of the pulses. The Ω_0 here can be set as its value with maximum overlap of the pulses, although it is usually evaluated by introducing the peak amplitudes for both pulses, as we will do in this paper. We can define a parameter

$$\xi_S \equiv \Omega_0\sigma \quad (7)$$

that measures the adiabaticity of the dynamics. In STIRAP, the adiabatic parameter is the averaged pulse area. The identifying feature of adiabatic passage via STIRAP is that the population in the wave function bridge is zero during the entire process, since $\Phi_0(x,t)$ is orthogonal to $\phi_b(x)$.

B. Molecular Geometry Considerations: Importance of the Wave Function Bridge. In this section we consider the practical problems of implementing and optimizing the STIRAP scheme in molecular systems, namely in the Na_2 dimer. Following the nomenclature and procedure of section 2, the initial state of the STIRAP system, $\phi_i(x)$, is now $\phi_0^X(x)$. We consider two different final states, $\phi_f(x) \equiv \phi_0^B(x)$ or $\phi_0^C(x)$, corresponding to two different STIRAP systems, the XAB system and the XAC system. The first problem consists of finding the best possible wave function bridge in the intermediate electronic potential, $\phi_b \equiv \phi_j^A(x)$, such that both μ_{ib} and μ_{bf} are as large as possible. In the Franck−Condon approximation, $\mu_{ib} \equiv p_{0j}^{XA} = \langle\phi_0^X(x)|\phi_j^A(x)\rangle$ and $\mu_{bf} \equiv p_{j0}^{AB} = \langle\phi_j^A(x)|\phi_0^B(x)\rangle$ (or equal to $p_{j0}^{AC} = \langle\phi_j^A(x)|\phi_0^C(x)\rangle$, depending on the target state selected). In Figure 2 we show the absolute value of the Franck−Condon amplitudes as a function of the intermediate state vibrational quantum number j. Also shown are the Franck−Condon amplitudes related to the overlap between $\phi_j^A(x)$ and adjacent states on the ground ($\phi_1^X(x)$) and final excited potentials ($\phi_1^B(x)$ and $\phi_1^C(x)$).

First consider Figure 2a. Due to the geometry of the three electronic potentials and a general reflection principle,[24] the repulsive part of the $V_A(x)$ curve is a mapping in the energy space of the spatial coordinate dependence of the vibrational wave functions of the ground electronic state, whereas the attractive part of $V_A(x)$ serves as a mapping of the vibrational wave functions of B $^1\Pi_u$. Since the role of the intermediate potential with respect to the ground and excited states is quite symmetrical, the mapping of the ground and excited wave functions in $V_A(x)$ greatly overlaps;[25] that is, many intermediate states can serve the purpose of a wave function bridge. The best compromise for having large Franck−Condon amplitudes in both transitions is obtained choosing $j = 10$, $\phi_{10}^A(x)$. Then, $p_{10}^{X,A} = 0.306$ and $p_{10,0}^{A,B} = 0.315$. The choice of a good wave

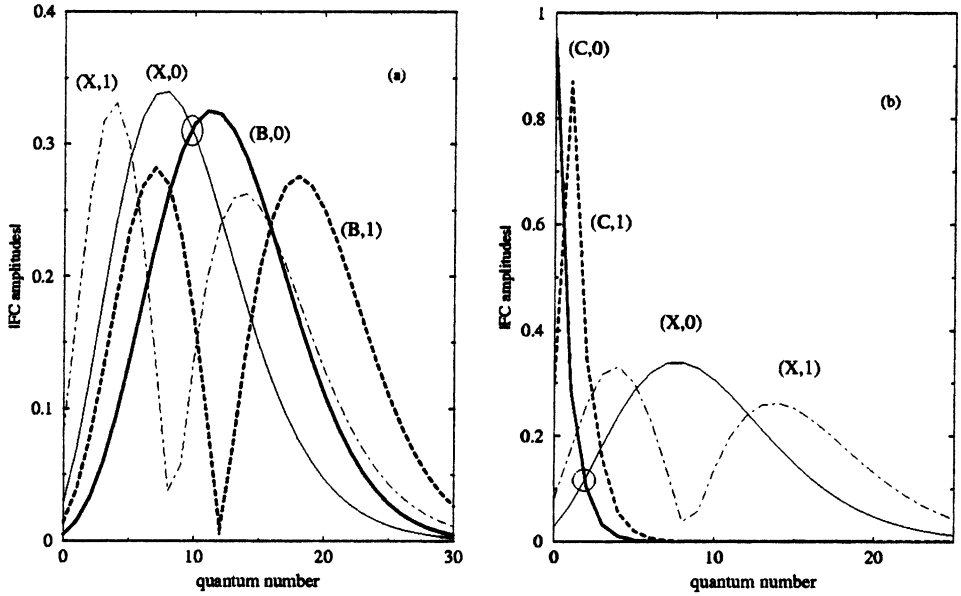

Figure 2. Absolute value of the Franck−Condon amplitudes for transitions involving different vibrational states of the intermediate electronic potential A Σ_u and a few vibrational states of the initial and target electronic potential. In the XAB system, the Franck−Condon amplitudes reflect the shape of the wave functions in the X Σ_g and B Π_g potentials by a reflection principle. However, in the XAC system the shape of the electronic potential C Σ_g is very similar to A Σ_u, so that the Franck−Condon amplitudes involving vibrational wave functions of A and C are approximately Dirac delta functions. For the overall two photon transition we must select a "good wave function bridge", that is, a single intermediate state that maximizes the Franck−Condon amplitudes for both transitions, between the initial state and the intermediate state, and between the intermediate state and the target state. In the XAB system this is achieved with the encircled state (A,10). In the XAC system the best wave function bridge corresponds to state (A,2) but involves quite smaller Franck−Condon amplitudes than in the previous system.

function bridge is decisive in reducing the amplitudes of nonresonant paths that break the adiabaticity and selectivity of STIRAP.[22]

In Figure 2b we show the absolute value of the Franck−Condon amplitudes corresponding to the XAC system. The geometry of the potential $V_C(x)$ is very similar to that of $V_A(x)$. Therefore, transitions between both electronic states are intrinsically quite selective, implying conservation of the vibrational quantum (A, v) → (C, v). The mappings of $\phi_0^X(x)$ and $\phi_0^C(x)$ on $V_{\Sigma_u}(x)$ almost do not overlap, and it is difficult to find a good wave function bridge. The best compromise is obtained for $j = 2$. Then, $p_{0,2}^{XA} = 0.123$ and $p_{2,0}^{AC} = 0.103$. The Franck−Condon amplitudes are 3 times smaller than in the previous case. More importantly, the Franck−Condon amplitudes of unwanted adjacent transitions, although nonresonant, are larger and therefore make their related transitions geometrically more favorable than the transitions involved in the STIRAP path.

C. Results of Population Transfer via STIRAP in Na_2. In Figure 3a we show the population histories for the STIRAP dynamics in the XAB system. We use two pulses of Gaussian shape with time width $\sigma = 1.5$ ps and maximum amplitudes $\epsilon_1^0 = \epsilon_2^0 = 5 \times 10^{-4}$ au, corresponding to a peak intensity of 9 GW/cm^2. The time delay between the pulses is $2\tau = 2.5$ ps. For these parameters we can estimate an adiabatic parameter $\xi_S = \sigma\sqrt{(\epsilon_1^0 p_{0,10}^{XA})^2 + (\epsilon_2^0 p_{10,0}^{AB})^2} \sim 12.7$, which corresponds approximately with an effective pulse area of 4π. Full population passage to (B,0) takes place with minor temporary excitation of the intermediate state. This result is in perfect agreement with the theory of STIRAP and indication that the 3-level Hamiltonian model can accurately describe the dynamics of the system in this regime. Reasonably good adiabatic population transfer is even possible with femtosecond pulses, with $\sigma = 600$ fs. Only for larger fields the Rabi frequency of competing processes can exceed the energy difference between (A,11) and (A,10), breaking the population locking condition and leading to Rabi oscillations of population to and from the wave function bridge.[22]

In Figure 3b−d we show the results of implementing STIRAP in the XAC system, using pulses with the same width and time delay as before. In case (b) the amplitude of the pulses is chosen so that the effective pulse area is also 4π. This case should yield similar results as the previous one if the 3-level Hamiltonian model were adequate to describe the dynamics of the system. However, the population dynamics follows a completely different behavior. First, there is population passage to the intermediate state (A,3), which is not the selected wave function bridge. Second, almost no population is transferred to the target wave function. Finally, there is some excitation of several levels in every electronic state.

The origin of the failure in the adiabatic passage stems from the poor Franck−Condon factors associated with the best-available wave function bridge, (A,3). Since the Franck−Condon amplitudes are 3 times smaller than those for the XAC system and $\xi_S = \sigma\sqrt{(\epsilon_1^0 p_{0,2}^{XA})^2 + (\epsilon_2^0 p_{2,0}^{AC})^2}$, to conserve the effective pulse area the amplitude of the pulses must be approximately 3 times larger than before. This amplitude enables nonresonant paths that, although not energetically favored, are geometrically preferred. The main source of instability in the STIRAP scheme is associated with changes in the sign of the Franck−Condon amplitudes of adjacent transitions. Indeed, in the limit of degenerate intermediate states with dipole moments of opposite sign, it is not possible to prepare the adiabatic dark state $\Phi_0(x,t)$ that drives the population in STIRAP.[26]

There are no good STIRAP solutions for the XAC system using pulses with 1.5 ps time widths. In Figure 3c we show the best possible result. This corresponds with using pulses of approximately the same intensity as in the XAB system, which in our case implies an effective area of only 1.5π, clearly below the threshold of adiabatic passage. For this area, the dynamics

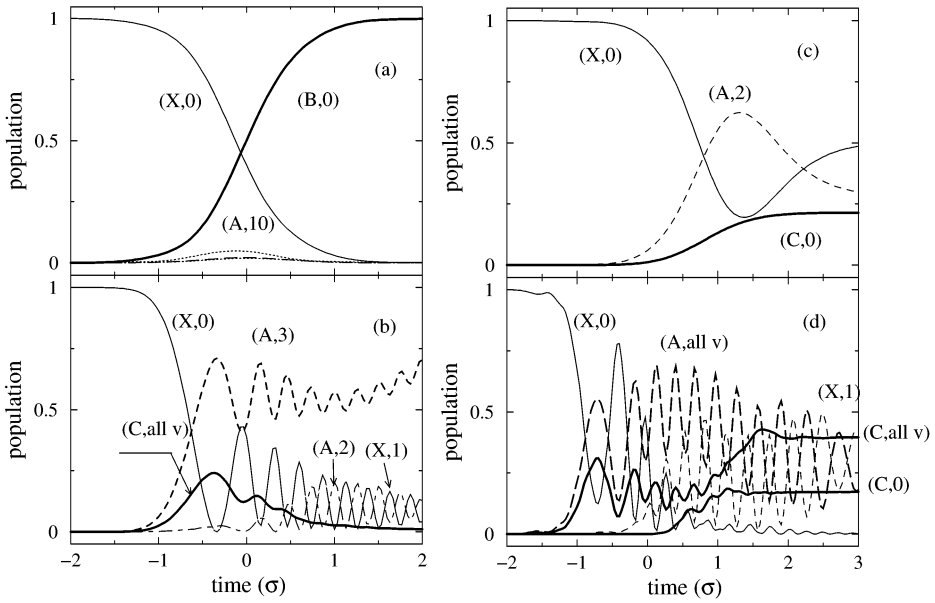

Figure 3. Population histories of the most important states participating in the dynamics of a STIRAP process for the XAB system (a) and the XAC system (b−d). In the XAB system, perfect STIRAP behavior is possible from (X,0) to (B,0) via the (A,10) state, using pulses with approximate pulse area $\xi_S \sim 4\pi$ and 1.5 ps time widths. In the XAC system, the Franck−Condon amplitudes are smaller even for the best wave function bridge. Therefore, to have $\xi_S \sim 4\pi$ (Figure 2b) the amplitudes of the pulses must be larger, enabling other transitions. The adiabatic transfer state is no longer orthogonal to the intermediate state, which is highly populated, stopping the passage to the target state. The 3-level Hamiltonian provides only a valid representation of the dynamics for smaller pulse areas, like $\xi_S \sim 1.5\pi$ in Figure 2c, before the threshold of adiabatic passage. Increasing the pulse area, like $\xi_S \sim 7.5\pi$ in Figure 2d does not restore the adiabaticity requirements.

of the 3-level Hamiltonian model reproduce well the dynamics in Na_2 (which are obtained solving eq 2). This fact indicates that the dynamics is selective, although only 20% of population is now transferred to the target state and the intermediate state is populated. The adiabaticity cannot be improved by increasing the amplitudes of the fields, as Figure 3b,d shows. In case (d) the effective area corresponds to 7.5π. The population transferred to the target state increases with respect to the 4π area, but the dynamics is clearly not selective nor robust under changes in the pulse parameters; i.e., the process is no longer adiabatic. The STIRAP dynamics can only be observed by using much longer laser pulses, with time widths of the order of 30 ps.

IV. From the Adiabatic to the Strong-Adiabatic Regime

STIRAP is a very general and powerful scheme, and we have seen that it can be implemented in molecular systems even in the subpicosecond regime. Physical bounds can be approximately framed by the conditions $\xi_S \geq 10$ (the exact number depending upon the system and pulse shape) and $\Omega_0 < \omega_v$, where we identify ω_v as the vibrational quantum in any of the potentials implied, although, as we have seen, the energy separation of levels in $U_2(x)$ is the main concern. Beyond that limit the simple assumptions of the model break. Not only do other states become accessible, thus reducing the selectivity of the scheme, but the population no longer flows via a single adiabatic dark state.

However, recently it has been observed that adiabatic passage can be recovered using much more intense pulses, in what we call a strong-adiabatic regime. The mechanism of population transfer is different and the method that exploits and generalizes its properties has been named APLIP. We analyze its features in the following sections. Figure 4 summarizes all the results of efficiency and selectivity of population passage as a function of the field amplitude (parametrized by $E_0 = \sqrt{(\epsilon_1^0)^2+(\epsilon_2^0)^2}$) for different time scales and final electronic potentials. Figure 4a,c,e shows the results for the XAB system using Gaussian pulses with time widths $\sigma = 6$, 1.5, and 0.6 ps, respectively, while Figure 4b,d,f shows the results for the XAC system using the same set of pulses as before. The properties of population transfer are monitored by following the population in the target vibrational state at final time, the electronic population in the target electronic state at final time (so that proximity of both curves measures the selectivity of the method), and the time-averaged population in the intermediate electronic state, $\langle P_A \rangle = \int_0^t dt' |\langle \psi_A(x,t') | \psi_A(x,t') \rangle|^2/\sigma$. Also shown are results of population transfer when the process is performed out of resonance; that is, when the lasers are tuned 0.014 au ($\sim$3100 cm^{-1}) above the resonance with the intermediate potential, all other parameters remaining the same. These conditions will be revealed to be particularly important when we analyze population passage via APLIP in the strong-adiabatic regime.

Let us start analyzing the results for larger time widths ($\sigma =$ 6 ps, $\tau = 10$ ps) in the XAB system. Inspection of the results of Figure 4a show the expected behavior of STIRAP for lower field amplitudes. Once the adiabatic requirement is fulfilled, the method is highly efficient and selective and its signature is clearly noticed as the drop in $\langle P_A \rangle$ reveals a dark resonance process (no fluorescence). For larger values in E_0 the population in the intermediate state is no longer locked and the population does not reach the final electronic state. However, as the field amplitude is further increased, the STIRAP scheme seems to gain some efficiency, although now the population transfer is not selective and is very sensitive to the exact value of E_0; that is, the method is no longer adiabatic. Finally for even stronger fields, the method recovers its previous efficiency and selectivity. Despite using strong fields tuned in resonance with transitions to intermediate states, the average population in $V_A(x)$ also decreases as if it were locked. Moreover the results can be improved by tuning both lasers off resonance with respect to

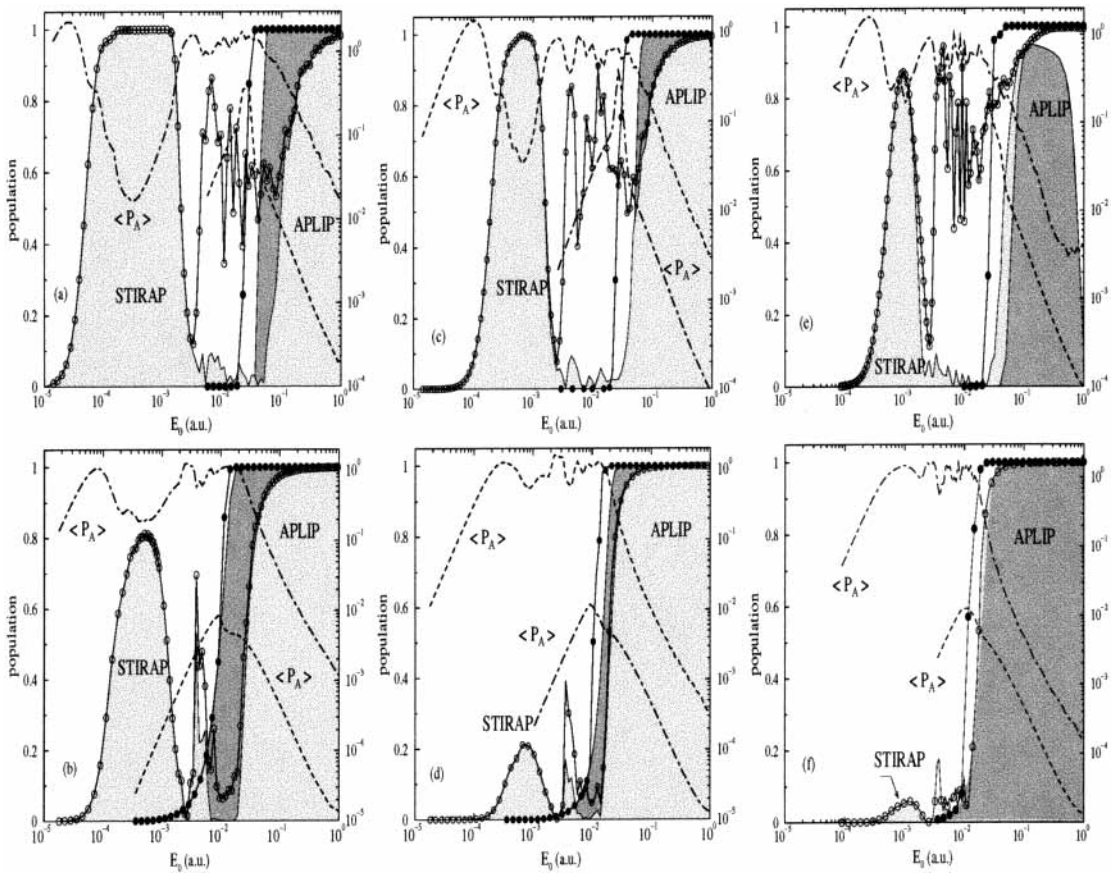

Figure 4. Efficiency and selectivity of the two-photon transfer as a function of the effective field amplitude E_0, for different pulse time widths and different target states. The curve with open circles represents the final population on the target electronic state for the resonant STIRAP-type transition, and the light gray shaded curve gives the population on the target vibrational state (selective transition) at final times. The time-averaged population on the intermediate electronic state, $\langle P_A \rangle$, is given by the dot−dashed curve, whose logarithmic scale is represented at the right side of the plot. At the top row are shown the results for the XAB system, while at the bottom row are the results for the XAC system. From left to right the time widths of the pulses change as $\sigma = 0.6$, 1.5, and 6 ps. For the XAB system STIRAP is possible in all the time widths tested, while only some STIRAP transfer (yield of ∼0.8) is possible for the larger time widths in the XAC system. Nearly in all cases the limit for adiabatic passage via STIRAP is around $E_0 \sim 10^{-3}$ au. On the other hand, APLIP is always possible in the XAC system but fails for very short time widths in the XAB system. Also the threshold of adiabatic passage via APLIP starts at larger E_0 in the XAB system than in the XAC system. Therefore, the transition from STIRAP to APLIP requires a smaller increase in pulse area in the XAC system. Except for very short pulse time widths, the performance in APLIP can be improved by detuning the lasers with respect to any intermediate state. The solid circles and the dark gray shaded curves provide respectively the overall population in the target electronic state and in the target vibrational level (selective transition) at late times for detuning $\Delta = 0.014$ au to the blue of the resonance with the intermediate level. The dashed line represents $\langle P_A \rangle$.

$V_A(x)$. This is the regime of strong-adiabatic transfer, where the population transfer follows the APLIP properties.

The same qualitative features in the population transfer are observed in Figure 4b for the XAC system. The STIRAP passage is not as perfect as in the previous case, and a maximum of 80% yield is obtained. The average population in the intermediate state is not so small, showing that the dark resonance is not perfect. This is because the Franck−Condon factors for the best wave function bridge found are clearly smaller than those for the XAB system, so that stronger pulses are required to obtain essentially the same pulse area as before. As in the discussion of the previous section, before reaching the threshold for successful population transfer, the Rabi frequency of the nearest off-resonant path becomes larger than the detuning, so that both paths interfere and destroy the dark resonance. For higher pulse intensities, in the strong-adiabatic regime, the population passage is however perfect, since is not affected by fine details in the adiabatic transfer state. On the contrary, although the Franck−Condon factors are smaller (at least for the intermediate state that is on resonance), the threshold of APLIP appears at lower amplitudes than in the XAB system. The difference between STIRAP and APLIP is smaller for this geometry of the potentials.

Figure 4c−f shows how the threshold for population transfer changes for both STIRAP and APLIP as the time width of the pulses (and therefore the time scale of the transfer) is reduced. In STIRAP, according to eq 7, a decrease in time leads to a linear increase in Ω_0 and therefore in E_0. For the XAB system even with subpicosecond pulses ($\sigma = 600$ fs) adiabatic passage via STIRAP yields almost 85%. The best result is obtained before the threshold of full adiabatic passage, so that the population is not perfectly locked in the wave function bridge. But for larger intensities, destructive interference with parallel paths destroys the adiabatic passage. In the XAC system of course, STIRAP is not possible for shorter pulses. On the other hand, the threshold for adiabatic passage via APLIP is almost independent of the time scale of the process, at least if the pulses are long enough so that the dynamics can still be considered adiabatic from the kinetic point of view. The APLIP dynamics can be achieved with subpicosecond pulses, especially in the XAC system. The dependence of APLIP and STIRAP with respect to the geometry of the potentials is thus very different.

V. Population Inversion in Molecular Systems via APLIP

A. Population Inversion in Molecular Systems via APLIP. To analyze features of the APLIP dynamics, Figure 5 shows the population histories for both the XAB and XAC systems, using pulses with $\sigma = 1.5$ ps, $\tau = 2.5$ ps, and $E_0 = 0.1$ au. The frequencies are detuned to the blue of the resonance with the intermediate state by 0.014 au. Now the Rabi frequencies for many different paths greatly exceed the energy difference from the resonance, so that many vibrational levels of the ground and final electronic potentials are excited. However, the overall dynamic picture remains very simple. In Figure 5a we observe the characteristic pattern of the APLIP dynamics. First, the population is mainly excited to high vibrational levels in the ground potential by means of Raman Stokes processes (although nonselective two-photon absorption is also present); this is rapidly followed by two-photon absorption from these levels to highly excited vibrational levels of the final potential; finally, by selective two-photon deexcitation (at some point similar to Raman anti-Stokes processes) all the population is driven to the target state, (B,0).

Using exactly the same laser parameters we observe qualitatively similar results for both systems. The transient excitation of highly excited vibrational levels in the ground and target electronic potentials is smaller for the XAC system. The effective time required to complete the population transfer is also smaller in this case. In the next section we will explain this feature on the basis the properties of the adiabatic passage via APLIP. In general, the APLIP dynamics is clearly less sensitive than STIRAP in regard to the geometry of the potentials. Similar results are also found using shorter or longer pulse time widths, as Figure 4 shows. Therefore, the adiabatic threshold of the APLIP dynamics is also weakly dependent on the pulse duration.

B. APLIP Mechanism. The simplest explanation of the physical mechanism of APLIP is based on the concept of light-induced potentials (LIPs). The basic Hamiltonian required to understand the APLIP dynamics includes three electronic potentials, as in eq 2,

$$\mathscr{H}_{\mathrm{APLIP}} = -\frac{\hbar}{2m}\frac{\partial^2}{\partial x^2}\mathscr{I} + \begin{pmatrix} U_1(x) & -\hbar\Omega_1(t)/2 & 0 \\ -\hbar\Omega_1(t)/2 & U_2(x) & -\hbar\Omega_1(t)/2 \\ 0 & -\hbar\Omega_2(t)/2 & U_3(x) \end{pmatrix} \quad (8)$$

The LIPs are the adiabatic (or dressed) potentials obtained by diagonalizing the part of the Hamiltonian comprising the electronic potential curves and laser couplings (the matrix in eq 8).

The mathematical formalization proceeds by finding the proper transformation matrix, $\mathscr{R}_a(x,t)$, such that the Schrödinger equation for the adiabatic wave functions

$$\mathrm{i}\hbar\frac{\partial}{\partial t}\vec{\Phi}^{\mathrm{A}}(x,t) = \left[-\mathscr{R}_a^{-1}(x,t)\frac{\hbar^2}{2m}\frac{\partial^2}{\partial x^2}\mathscr{R}_a(x,t) + \mathscr{U}^{\mathrm{LIP}}(x,t) - \mathrm{i}\mathscr{R}_a^{-1}(x,t)\frac{\partial}{\partial t}\mathscr{R}_a^{-1}(x,t)\right]\vec{\Phi}^{\mathrm{A}}(x,t) \quad (9)$$

where $\vec{\Phi}^{\mathrm{A}}(x,t) = (\Phi_+(x,t),\Phi_0(x,t),\Phi_-(x,t))^\dagger = \mathscr{R}_a^{-1}(x,t)(\psi_1(x,t),\psi_2(x,t),\psi_3(x,t))^\dagger$ is the diagonal in the potential energy matrix $\mathscr{U}^{\mathrm{LIP}}(x,t)$. If the initial wave function is placed on a single LIP, then it will move under the influence of a single potential. There are two terms that conspire against the adiabatic motion of the wave packet, transferring population among different LIPs and changing the shape of the wave packet. These are the first and the last terms in the right-hand side (RHS) of eq 9. Usually, the first term is referred to as the spatially nonadiabatic term, and the last one, as the temporally nonadiabatic term.[20] For a 3-electronic state system the LIPs are labeled for decreasing order of energy as $\{U_+(x,t), U_0(x,t), U_-(x,t)\}$. Both $\mathscr{R}_a(x,t)$ and $\mathscr{U}^{\mathrm{LIP}}(x,t)$ have analytical expressions, but their forms are too complicated to facilitate understanding of the process.

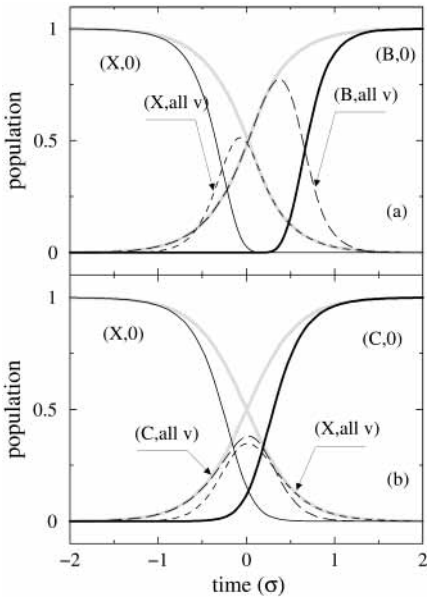

Figure 5. Population histories of the most important states participating in the dynamics of an APLIP process for the XAB system (a) and the XAC system (b). In both cases the pulse parameters are the same. Population transfer via APLIP requires substantial vibrational excitation in the ground and target electronic states at intermediate times, although the A Σ_u electronic state is barely populated. This transient excitation is larger in the XAB system than in the XAC system.

To gain insight into the mechanism of APLIP, we show in Figure 6 a pictorial sketch of how the LIPs look as the pulses vary in time. Notice that the potentials here are shifted by the energy of the photons, in the spirit of the RWA, $U_1(x) = V_1(x)$, $U_2(x) = V_2(x) - \hbar\omega_1$, and $U_3(x) = V_3(x) - \hbar(\omega_1 + \omega_2)$.

The initial wave function is in $U_1(x)$, which, according to Figure 6, correlates with the left well of $U_0^{\mathrm{LIP}}(x,t)$. The overall APLIP process consists of moving this wave function to the right well, where it correlates with $U_3(x)$. Therefore, the physical mechanism of the adiabatic passage requires the elimination of the internal barrier, E_{bar}, that separates both wells in $U_0^{\mathrm{LIP}}(x,t)$, at a certain time. The scheme of Figure 6 shows how this occurs using a counterintuitive sequence of pulses blue-detuned with respect to $V_2(x)$. At time t_1 the amplitude of the second pulse, $\epsilon_2(t)$, is large, strongly coupling $U_2(x)$ with $U_3(x)$. By dynamic Stark shift the energy difference between both potentials increases, so that the right well of $U_0^{\mathrm{LIP}}(x,t)$ is elevated and the internal energy barrier increases. The first pulse $\epsilon_1(t)$ causes a similar Stark shift on $U_1(x)$ which raises the energy of the left well of $U_0^{\mathrm{LIP}}(x,t)$. Therefore, as $\epsilon_2(t)$ decreases and $\epsilon_1(t)$ increases there is an interval of time around t_2 where the internal energy barrier is suppressed, allowing the displacement of the wave packet. Finally $\epsilon_1(t)$ decreases as well, so that the energy barrier is recovered and the wave packet cannot recross. During the entire time evolution $U_-^{\mathrm{LIP}}(x,t)$ behaves approximately like $U_2(x)$, except for overall shifts in energy caused by the dynamic Stark effects.

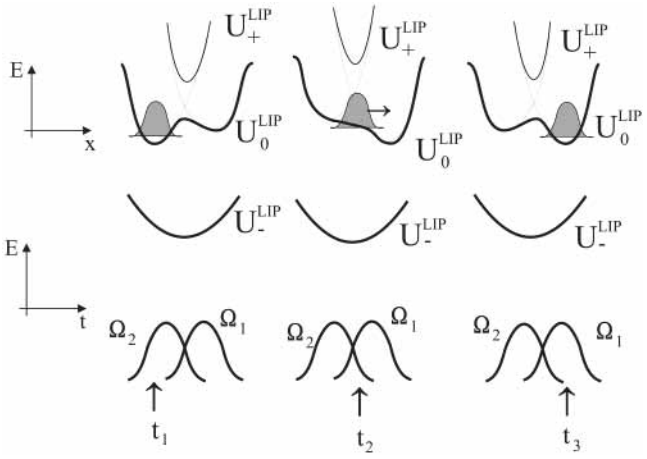

Figure 6. Scheme of the mechanism of population transfer via APLIP. The cartoon shows the LIPs at three different times. The wave packet moves in the initial LIP, U_0^{LIP}, that has an internal barrier that prevents the crossing of the wave packet from the left well corresponding to the initial configuration, $V_1(x)$, to the right well corresponding to the target configuration, $V_3(x)$. At intermediate times U_0^{LIP} shows no internal barrier allowing the motion of the wave packet to the desired final position.

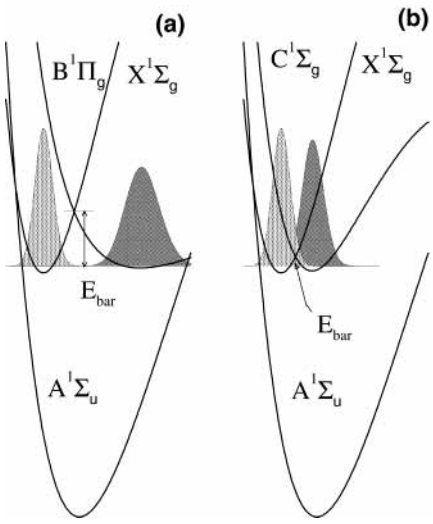

Figure 7. Energy-shifted electronic potentials in the diabatic representation showing the energy barrier that the initial wave function must surmount to move along the bond distance before reaching the desired state. In the XAB system (a) the energy barrier and the separation between the equilibrium positions is much larger than in the XAC system (b), where the initial and final wave functions partially overlap.

The motion of the wave packet from the left well to the right well implies the sequence of dynamical processes that we observe in the population histories. First the wave packet overlaps higher vibrational levels in $U_1(x)$, then it overlaps higher vibrational levels in $U_3(x)$, and finally the wave packet stops at the equilibrium position in $U_3(x)$. The selection of the ground vibrational level in $U_3(x)$ is guaranteed if the dynamics is both temporally and spatially adiabatic, so that the shape of the wave packet (its number of nodes) is not distorted.

C. Adiabatic Thresholds in APLIP: Geometry Considerations. As observed in the results of Figure 4, there is an energy gap between the region where STIRAP works and the region where APLIP is effective. The threshold for APLIP depends on the geometry of the potentials but is not very sensitive with respect to changes in the pulse durations. It is therefore obvious that different adiabatic requirements must be found to adequately describe the APLIP transfer. In principle, a thorough examination of nonadiabatic couplings[27] induced by the kinetic term and the time-dependent term in eq 9 is needed to derive a single (or multiple) parameter ξ_A that replaces the STIRAP condition ξ_S. This procedure cannot be performed analytically without approximations. Here we will follow a simpler physically motivated model that reflects some of the adiabatic requirements of the method, allowing for a simple parametrization of ξ_A.

Let us follow the displacement of the vibrational population along the bond distance, from the minimum in $U_1(x)$ to the minimum in $U_3(x)$. In Figure 7 we show the electronic states dressed with the photon energies for both the XAB and XAC systems. In order that the wave function can reach the equilibrium position in $U_3(x)$, the pulses must temporally provide an energy larger than the energy barrier that separates both minima. This stage corresponds to the Raman Stokes processes that initiate the dynamics. In the XAB system, the internal barrier $E_{bar} \sim 640$ cm^{-1}, which implies that the wave packet must gain in average four vibrational quanta in the Raman process to overcome the barrier. In the XAC system, $E_{bar} \sim 110$ cm^{-1}, so that only one vibrational quantum is necessary to overcome the barrier. Indeed the initial and final wave functions partially overlap, so that the probability for a two-photon Franck−Condon transition is not zero. When both pulses fully overlap, the effective two-photon Rabi frequency Ω_{eff} must be larger than E_{bar}, allowing the wave packet to move from one potential to the other, which is signaled as a two-photon absorption process. Finally, as the pulses are switched off, the transient energy disappears, and by two-photon resonance the wave packet ends up in the bottom of $U_3(x)$. Since in APLIP the whole wave function is transferred from one potential to the other, the energy demands for adiabatic passage will depend on the displacement of the wave packet along the bond distance that is required to reach the final equilibrium configuration. For highly non-Franck−Condon transitions, as in the XAB system, we expect larger adiabatic requirements than for more "vertical" type transitions.

We will now assume that the wave packet is a classical particle moving from the minimum in $U_1(x)$ to $U_3(x)$ at speed v_c. The laser coupling via the effective Rabi frequency Ω_{eff} must provide the kinetic energy so that the particle overcomes the barrier. A Landau−Zener model gives the probability of crossing the barrier, which is[12]

$$P_{U_1 \to U_3} \approx 1 - \exp(-\pi \Omega_{eff}^2/2\alpha) \tag{10}$$

with

$$\alpha = \left| \frac{v_c}{2\hbar} \frac{d(U_3 - U_1)}{dx} \right|_{x=x_c} \tag{11}$$

where x_c is the crossing point. We assume that the process of crossing the barrier adequately describes the adiabatic passage of the wave packet to the final electronic state. The adiabatic parameter of APLIP is therefore proposed as $\xi_A = \Omega_{eff}^2/2\alpha$.

The parameter α can be approximately evaluated in several ways. For example, if we consider that $U_1(x)$ and $U_3(x)$ are

displaced harmonic potentials with the same fundamental frequency, ω, then

$$\frac{\mathrm{d}}{\mathrm{d}x}|U_3(x) - U_1(x)| = m\omega^2 d \tag{12}$$

where m is the reduced mass of the molecule and d is the distance between the potential minima. In other cases we will use the average frequency of the potentials involved. Since we assume that the kinetic energy must be larger than the energy barrier, $v_c > (2E_{bar}/m)^{1/2}$. Substituting $d = \sqrt{8E_{bar}/m\omega^2}$, we obtain $\alpha \sim 2\omega E_{bar}/\hbar$.

In this model the detuning of the intermediate potential is needed to avoid the crossing of the potentials $U_1(x)$ and $U_3(x)$ by $U_2(x)$ in the course of the particle's trajectory. This is achieved if the absolute value of the detuning $|\Delta|$ is made at least larger than E_{bar}. The model cannot explain the avoided crossing with $U_2(x)$ in resonant conditions, since it does not incorporate quantum effects as those in the STIRAP dynamics. For almost resonant conditions, such that $\Omega_1(t_c),\Omega_2(t_c) \gg |\Delta|$, the effective Rabi frequency is approximately Ω_0. (These are the conditions that we are exploring in this paper.) Summing up the pieces, we obtain for the adiabatic parameter

$$\xi_A = \frac{\Omega_{eff}{}^2\hbar}{4E_{bar}\omega} \tag{13}$$

Although the expression for ξ_A does not depend on the time duration of the pulses, we will still call ξ_A an effective pulse area, to be compared with that of the STIRAP process.

We analyze now whether eq 13 describes correctly the adiabatic features of APLIP. We can fix a particular final probability in the target electronic state, for example $P_3 \gtrsim 0.95$, to specify the threshold of adiabaticity in APLIP dynamics. From the results of Figure 4 we obtain the values of Ω_0 (which is E_0 for APLIP in the Franck−Condon approximation) that correspond to that choice of threshold, $\Omega_0(P_3 \gtrsim 0.95)$. For the nonresonant case ($|\Delta| = 0.014$ au) we obtain in the XAB system $\Omega_0(P_3 \gtrsim 0.95) \sim 0.030$, 0.032, and 0.031 au for $\sigma = 0.6$, 1.5, and 6 ps, respectively. In the XAC system we obtain $\Omega_0(P_3 \gtrsim 0.95) \sim 0.017$, 0.014, and 0.014 for the same set of pulses. It is observed that $\Omega_0(P_3 \gtrsim 0.95)$ is larger in the XAB system, which has a larger energy barrier E_{bar} than in the XAC system, while the results are not very sensitive to the duration of the pulses. Assuming that $\Omega_{eff} \approx \Omega_0$ and using eq 13, we obtain $\xi_A \sim 50\pi$ for all of the results, showing good qualitative agreement.

Quantitatively, the values of ξ_A are overestimated if we consider them to be effective pulse areas. Given that the population transfer is still not perfect, we could expect ξ_A to be of the order of $2-3\pi$, using the same criteria as in the STIRAP case. The overestimation is due to several reasons. First, since $\Delta \approx \Omega_0$, the effective two-photon Rabi process does not correspond to that of a truly resonant process, and actually $\Omega_{eff} < \Omega_0$. Another reason is that in the derivation of eq 13 we estimate α assuming the minimum possible kinetic energy for the particle.

There are two more features of the adiabatic passage that are correctly described by eq 13, at least in a qualitative way. The first one is the quadratic dependence of ξ_A with respect to Ω_0, $\xi_A \propto \Omega_0{}^2$. This fact explains why the yield of population transfer in the onset of the adiabatic threshold increases much faster in APLIP than in STIRAP, where $\xi_S \propto \Omega_0$ (see Figure 4). The second one is the dependence of ξ_A with respect to the required displacement of the population along the bond distance in order to reach the target state. Assuming harmonic oscillators and substituting E_{bar} in terms of the spatial distance between the initial and final equilibrium positions, d, we obtain

$$\xi_A = \frac{2\Omega_{eff}{}^2\hbar}{m\omega^3 d^2} \tag{14}$$

Fixing a specific yield for the final population in the target electronic state (for instance $P_3 \gtrsim 0.95$) amounts to fixing the adiabatic requirements, so that we obtain a linear relation between the threshold Rabi frequency and the distance between the potentials,

$$\Omega_{eff}(\xi \gtrsim P_3) \propto d \tag{15}$$

In Figure 8 we show how $\Omega_0(P_3 = 0.95)$ changes as a function of d for population passage via APLIP in a model of displaced harmonic oscillators with the same frequencies. We have chosen a negative detuning, $\Delta = -0.02$ au, for the second potential, and we have assumed that $\Omega_{eff} \approx \Omega_0$. The results show that the relation between Ω_0 and d is only approximately linear. As we will show in the next section, as d approaches zero, the APLIP dynamics converges into the STIRAP dynamics, so that ξ_A does not give the correct limit. Finally, the results also depart from linearity for large values of d. This can be expected since the adiabatic parameter derived in our simple model depends essentially on the adiabatic properties at the crossing between the $U_1(x)$ and $U_3(x)$ potentials (that is, on the two-photon absorption process). As the distance between the potentials increases, the whole APLIP process is dominated by the motion of the wave packet on each potential (that is, on the Raman processes), so that the adiabatic parameter should be derived in terms of specific adiabatic requirements imposed on the Raman processes.[26]

Previously we have estimated ξ_A in terms of a Rabi frequency obtained for threshold values of population transfer to the target electronic state, $\Omega_0(P_3)$. The qualitative agreement of ξ_A with the numerical results is poorer if we base the calculation on thresholds for selective adiabatic population transfer to the target vibrational state, P_f. In Figure 4 we observe that $\Omega_0(P_{3,v=0})$ depends more sensitively than $\Omega_0(P_f)$ on the duration of the pulses. For larger pulses, $\Omega_0(P_{3,v=0})$ is closer to $\Omega_0(P_3)$ than for shorter pulses. The proposed simple model, based on a classical motion of a particle, cannot yield insight into the adiabatic requirements for selectivity in APLIP. For the resonant case ($\Delta = 0$) the qualitative agreement is also poorer, since the model requires a detuning to explain the correct adiabatic passage.

D. Quasi-Adiabatic Description. A more quantitative picture of the APLIP process can be obtained by applying the rotation matrix $\mathscr{R}_s(t)$, which diagonalizes the STIRAP Hamiltonian (see eq 3), to the APLIP Hamiltonian. By this procedure we analyze APLIP in the natural representation of the STIRAP dynamics. Assuming that the Rabi frequencies are not dependent on position (the Franck−Condon approximation) we obtain the Schrödinger equation

$$i\hbar\frac{\partial}{\partial t}\vec{\Phi}^{QA}(x,t) = -\frac{\hbar^2}{2m}\frac{\partial^2}{\partial x^2}\mathscr{R}\vec{\Phi}^{QA}(x,t) + \mathscr{V}^{QA}(x,t) - i\mathscr{R}_s{}^{-1}(t)\frac{\partial}{\partial t}\mathscr{R}_s(t)\vec{\Phi}^{QA}(x,t) \tag{16}$$

where

$$\mathscr{U}^{QA} = \frac{1}{2}\begin{pmatrix} U_1 \sin^2\theta + U_3\cos^2\theta + U_2 + \Omega_0 & \sqrt{2}(U_1 - U_3)\sin(2\theta)/2 & U_1\sin^2\theta + U_3\cos^2\theta - U_2 \\ \sqrt{2}(U_1 - U_3)\sin(2\theta)/2 & 2(U_1\cos^2\theta + U_3\sin^2\theta) & \sqrt{2}(U_1 - U_3)\sin(2\theta)/2 \\ U_1\sin^2\theta + U_3\cos^2\theta \text{ - } U_2 & \sqrt{2}(U_1 - U_3)\sin(2\theta)/2 & U_1\sin^2\theta + U_3\cos^2\theta + U_2 - \Omega_0 \end{pmatrix} \quad (17)$$

with $\theta(t) = \arctan(\Omega_1(t)/\Omega_2(t))$, the adiabatic mixing angle. In eq 17 the diagonal elements are the quasi-adiabatic LIPs (QAPs) that remain coupled because $\mathscr{R}_s(t)$ is not exactly appropriate to diagonalize the APLIP Hamiltonian. The initial quasi-adiabatic wave packets are obtained by $\vec{\Phi}^{QA}(x,0) = \mathscr{R}_s^{-1}(0)\vec{\psi}(x,0)$. By application of a counterintuitive sequence, it can be seen that

$$\Phi_0{}^{QA}(x,t) = \cos\theta(t)\psi_1(x,t) - \sin\theta(t)\psi_3(x,t) \quad (18)$$

so that for $t = 0$, $\Phi_0{}^{QA}(x,0) \approx \psi_1(x,0)$. The initial quasi-adiabatic wave packet lies in $U_0{}^{QAP}(x,t)$.[28] The mechanism of adiabatic passage in the quasi-adiabatic representation is based on the dynamic changes in $U_0{}^{QAP}(x,t)$,

$$U_0{}^{QAP}(x,t) = U_1(x)\cos^2\theta(t) + U_3(x)\sin^2\theta(t) = \frac{1}{\Omega_0(t)}(\Omega_2(t)U_1(x) - \Omega_1(t)U_3(x)) \quad (19)$$

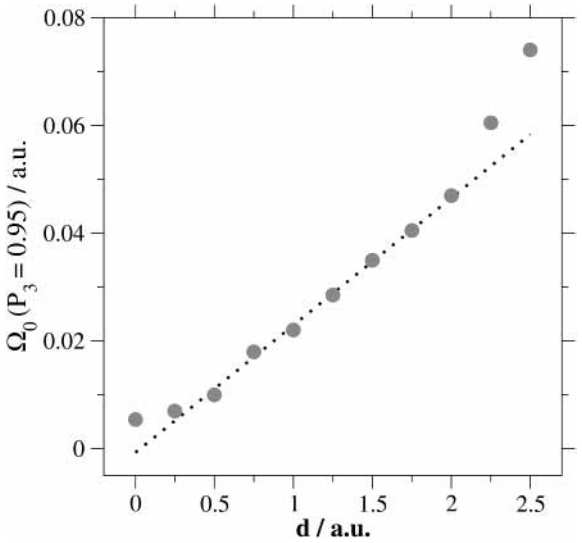

Figure 8. Dependence of the threshold of adiabatic passage in APLIP with respect to the distance between the equilibrium separations of the initial and target electronic states. As the distance between the nuclear configurations increases, the amplitude of the pulses must increase approximately linearly to ensure adiabatic passage. The results are obtained for a model system of three displaced harmonic oscillators.

In Figure 9 we represent $U_0{}^{QAP}(x,t)$ for the XAB case. The projection of the QAP shows the path followed by the quasi-adiabatic wave packet. The form of $U_0{}^{QAP}(x,t)$ approximately reproduces the electronic lever mechanism that allows the wave packet passage, as introduced before. Also $U_2(x)$ does not participate in the shaping of $U_0{}^{QAP}(x,t)$, so that $\Phi_0{}^{QA}(x,t)$ does not overlap with states of the intermediate potential.

In the quasi-adiabatic representation there are two sources for couplings that move the wave packet away from the minimum path in $U_0{}^{QAP}(x,t)$. The first one is the temporal nonadiabatic term (last term from eq 16). The second one is the "direct" coupling between the QAPs,

$$\mu_{0\pm}{}^{QA}(x,t) = \frac{\sqrt{2}}{4}\sin(2\theta)(U_1(x) - U_3(x)) = \frac{\sqrt{2}}{2}(U_1(x) - U_3(x))\frac{\Omega_1(t)\Omega_2(t)}{\Omega_0{}^2(t)} \quad (20)$$

This term is a consequence of choosing a simpler representation which does not diagonalize the APLIP Hamiltonian. It also incorporates the spatially nonadiabatic couplings in eq 9. The form of the coupling (eq 20) separates the temporal from the spatial contributions, facilitating the evaluation of its effects on the wave packet motion. It can be observed that $\mu_{0\pm}{}^{QA}(x,t)$ will be small at the positions and times where the amplitude of $\phi_0{}^{QA}(x,t)$ is large during the passage. For instance, at initial and final times $\Omega_1(t)\Omega_2(t) \approx 0$, while at intermediate times the wave packet is near the avoided crossing region x_c, where $U_1(x_c) \approx U_3(x_c)$, so that the coupling term, $\mu_{0\pm}{}^{QA}(x,t)$, is small.

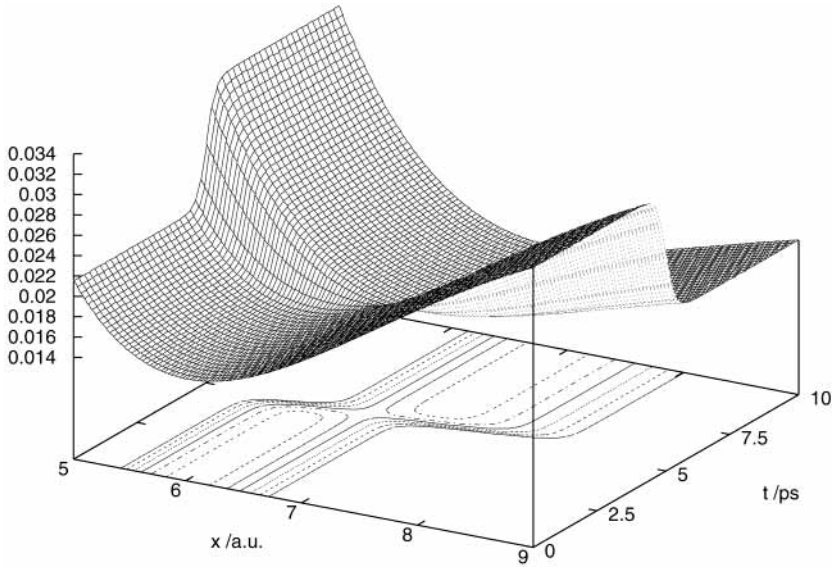

Figure 9. Structure of the quasi-adiabatic LIP, $U_0{}^{QAP}(x,t)$, that allows adiabatic passage via APLIP according to the quasi-adiabatic description.

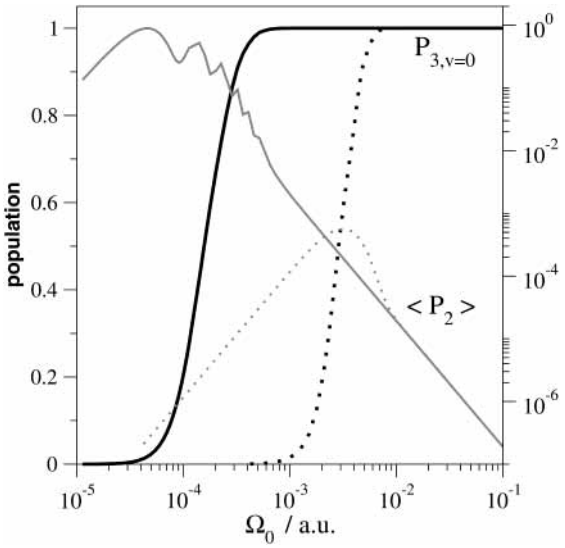

Figure 10. Population transfer between an initial and target electronic potentials of identical shape as a function of the pulse amplitudes E_0. The transfer is selective and robust at a threshold corresponding to the adiabatic requirements of STIRAP and is not limited as E_0 increases, so that the STIRAP and APLIP schemes converge. The final target population $P_{3,v=0}$ is almost unity for all E_0, and the time-averaged population in the intermediate electronic state $\langle P_2 \rangle$ drops linearly with E_0. The solid lines represent the results for resonant transfer with a vibrational level in the intermediate electronic state, while the dotted-line curves represent the results using a blue detuning of $\Delta = -0.02$ au. The same results are obtained with red detuning. The threshold of population transfer depend with detuning in a manner expected for nonresonant STIRAP. Otherwise the same results are obtained for different detuning as E_0 increases.

If both potentials have approximately the same shape and equilibrium configuration, then $\mu_{0\pm}^{QA}(x,t) = 0$ and $U_0^{QAP}(x,t) = U_0^{LIP}(x,t)$; that is, the quasi-adiabatic potential is indeed the light-induced potential. In this limit, of course, $U_0^{LIP}(x,t) = U_1(x) = U_3(x)$, so that there are no dynamics (displacements) in the spatial coordinate. The STIRAP and the APLIP method converge. This means that adiabatic passage happens for all pulse amplitudes E_0 larger than the adiabatic threshold for STIRAP, given by ξ_S (eq 7), for resonant conditions. The results for this hypothetical molecular scenario are shown in Figure 10, where we use the same harmonic potential curve for the ground and final target electronic state.

In general, if the couplings are weak, we can assume that there are no transitions between different QAPs, so that the wave packet follows the equation

$$i\hbar\frac{\partial}{\partial t}\Phi_0^{QA}(x,t) = \left[-\frac{\hbar^2}{2m}\frac{\partial^2}{\partial x^2} + U_0^{QAP}(x,t)\right]\Phi_0^{QA}(x,t) \quad (21)$$

The kinetic and potential operators can distort the shape of $\Phi_0^{QA}(x,t)$, but they do not change the different contributions of the electronic potentials provided by eq 18. Therefore, the electronic populations, $P_1(t) = \Omega_2^2(t)/\Omega_0^2(t)$ and $P_3(t) = \Omega_1^2(t)/\Omega_0^2(t)$, follow the same dynamical behavior as the vibrational state populations in STIRAP, a result observed in Figure 5.

Finally, we discuss the role of the detuning in the quasi-adiabatic representation. According to our model, the effect of the detuning is incorporated in $U_2(x)$, which is the energy shifted intermediate potential. Since $U_2(x)$ does not appear in $U_0^{QAP}(x,t)$ or in $\mu_{0\pm}^{QA}(x,t)$, it would seem that the detuning does not play any role in the APLIP process, which is not consistent with the numerical results.[18,20] The schematic picture of Figure 11 explains how the effects of the detuning can be incorporated in the quasi-adiabatic description. For blue detuning, the energy of $U_0^{QAP}(x,t)$ (or $U_0^{LIP}(x,t)$) is above the energy of $U_-^{QAP}(x,t)$ and below the energy of $U_+^{QAP}(x,t)$. As the amplitude of the field increases, by Stark shift these QAPs (or LIPs) separate from each other due to the $\pm\Omega_0(t)$ term in the equations (see eq 17). Then, $|U_0^{QAP}(x,t) - U_\pm^{QAP}(x,t)| \gg \mu_{0\pm}^{QA}(x,t)$, and the effect of the couplings can be neglected. The dynamics can be followed solely by eq 21. However, when the frequencies are detuned to the red of $V_2(x)$, at initial times the energy of $U_0^{QAP}(x,t)$ is also below the energy of $U_-^{QAP}(x,t)$. When the amplitudes of the fields increase, by Stark shift $U_-^{QAP}(x,t)$ will cross $U_0^{QAP}(x,t)$, so that the adiabatic couplings cannot be neglected even if $\mu_{0\pm}^{QA}(x,t)$ is as small as before. Now eq 21 does not provide an accurate description of the dynamics. The true LIP will actually look like $U_0^{QAP}(x,t)$ at initial and final times (before the nonadiabatic crossing) and like $U_-^{QAP}(x,t)$ at intermediate times. Moreover, during the crossings, the coupling induces spatial distortions in the wave packet.

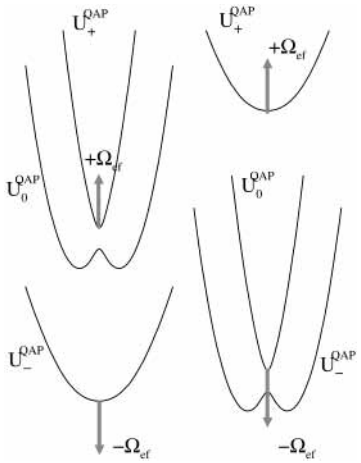

Figure 11. Schematic description of the role of detuning in STIRAP according to the quasi-adiabatic representation. Although U_0^{QAP} does not depend on detuning, for blue detuning U_0^{QAP} is always far from the other LIPs when the couplings, $\mu_{0\pm}^{QA}$, are important, so that the population is solely transferred in U_0^{QAP}. However, for red detuning U_-^{QAP} crosses with U_0^{QAP} both at the beginning and end of the process, therefore inducing nonadiabatic population transfer to U_-^{QAP}.

VI. Final Remarks

We have studied the control of vibrationally selective highly non-Franck−Condon electronic transitions by ultrafast laser pulses, as a function of the geometry of the electronic states and the intensity and duration of the pulses. We have explored the efficiency and robustness of an adiabatic passage scheme on the basis of a particular class of time delay control using a counterintuitive sequence of two laser pulses.

For moderate intensities, the scheme is generally named STIRAP and makes use of a resonant transition to an intermediate state that works as a "wave function bridge" between the initial and target states. The efficiency of the scheme can be estimated by a simple adiabatic condition, given by eq 1. However, the adiabatic condition is no longer useful in the strong intensity regime, where STIRAP dynamics is no longer selective or efficient for population transfer. For strong pulses the two-photon electronic transition can be controlled in a very robust way by another scheme, named APLIP, with many similar features. In previous contributions[18,20−22] we have studied the dynamics of APLIP and showed its performance using frequency detuned transitions and both counterintuitive and intuitive sequences. Here we propose a very simple model for APLIP

and we concentrate on the relations between both methods in terms of their adiabatic properties, following the dynamics for different electronic state geometries, time durations, and increasing pulse intensities. Whereas adiabatic following in STIRAP is based on the properties of a single adiabatic state and requires fine control on the Hamiltonian in the adiabatic representation, the APLIP dynamics is based on shaping the electronic potential in the adiabatic representation, requiring only a more "crude" or less detailed control.

By numerical simulations for two different vibronic transitions in Na_2 we have shown the areas where the STIRAP and APLIP schemes are efficient and selective. The range of efficiency of the STIRAP method is clearly revealed in our study and possible limitations are outlined. However, our results do not show the limitations in APLIP. These appear when we evaluate the validity of the model used in our calculations, which is based on a Hamiltonian with three-electronic potentials in the rotating wave approximation. For very strong laser fields this model does not include highly nonlinear phenomena observed in the dynamics, such as competing multiphoton transitions and autoionization. For some electronic geometries the threshold for population transfer in APLIP occurs already at the onset where the model breaks. Therefore, the utility of the APLIP scheme for more general systems will rely on our ability to extend the control in the modulation of the potentials for *n*-electronic states beyond the rotating wave approximation. The use of frequency chirped pulses assisted by optimal control techniques may become an important additional tool in the control of the dynamics. Work along these lines is in prospect.

Acknowledgment. Financial support from the Dirección General de Investigación Científica y Técnica under Project BQU2002-00173/ is gratefully acknowledged. I.R.S. also acknowledges financial support from the Ministerio de Educación y Ciencia for a postdoctoral fellowship and Prof. H. Rabitz for stimulating conversations. V.S.M. acknowledges financial support from the Michigan Center for Theoretical Physics and the FOCUS Center.

References and Notes

(1) Crim, F. F. *J. Phys. Chem.* **1996**, *100*, 12725.
(2) Rice, S. R.; Zhao, M. *Optimal control of molecular dynamics*; John Wiley & Sons: New York, 2000.
(3) Shapiro, M.; Brumer, P. *Adv. At. Mol. Opt. Phys.* **2000**, *42*, 287.
(4) Vitanov, N. V.; Halfmann, T.; Shore, B. W.; Bergmann, K. *Annu. Rev. Phys. Chem.* **2001**, *52*, 763.
(5) Oreg, J.; Hioe, F. T.; Eberly, J. H. *Phys. Rev. A* **1984**, *29*, 690.
(6) Gaubatz, U.; Rudecki, P.; Schiemann, S.; Bergmann, K. *J. Chem. Phys.* **1990**, *92*, 5363.
(7) Bergmann, K.; Theuer, H.; Shore, B. W. *Rev. Mod. Phys.* **1998**, *70*, 1003.
(8) Pierce, A. P.; Dahleh, M. A.; Rabitz, H. *Phys. Rev. A* **1988**, *37*, 4950.
(9) Kosloff, R.; Rice, S. A.; Gaspard, P.; Tersigni, T.; Tannor, D. J. *Chem. Phys.* **1989**, *201*, 139.
(10) Judson, R. S.; Rabitz, H. *Phys. Rev. Lett.* **1992**, *68*, 1500.
(11) Mitra, A.; Sola, I. R.; Rabitz, H. *Phys. Rev. A* **2003**, *67*, 043409.
(12) Garraway, B. M.; Suominen, K.-A. *Rep. Prog. Phys.* **1995**, *58*, 365.
(13) Bandrauk, A. D.; Aubanel, E. E.; Gauthier, J.-M. In *Molecules in Laser Fields*; Bandrauk, A. D., Ed.; Dekker: New York, 1994.
(14) Guisti-Suzor, A.; Mies, F. H.; DiMauro, L. F.; Charron, E.; Yang, B. *J. Phys. B* **1995**, *28*, 309.
(15) Frasinski, L. J.; Posthumus, J. H.; Plumridge, J.; Codling, K.; Taday, P. F.; Langley, A. J. *Phys. Rev. Lett.* **1999**, *83*, 3625.
(16) Garraway, B. M.; Suominen, K.-A. *Phys. Rev. Lett.* **1998**, *80*, 932.
(17) Solá, I. R.; Santamaría, J.; Malinovsky, V. S. *Phys. Rev. A* **2000**, *61*, 043413.
(18) Solá, I. R.; Chang, B. Y.; Santamaría, J.; Malinovsky, V. S.; Krause, J. L. *Phys. Rev. Lett.* **2000**, *85*, 4241.
(19) Rodriguez, M.; Suominen, K.-A.; Garraway, B. M. *Phys. Rev. A* **2000**, *62*, 053413.
(20) Chang, B. Y.; Solá, I. R.; Santamaría, J.; Malinovsky, V. S.; Krause, J. L. *J. Chem. Phys.* **2001**, *114*, 20.
(21) Malinovsky, V. S.; Krause, J. L. *Chem. Phys.* **2001**, *47*, 267.
(22) Solá, I. R.; Chang, B. Y.; Malinovsky, V. S.; Santamaría, J. In *Femtochemistry and Femtobiology*; Douhal, A., Santamaría, J., Eds.; World Scientific: Singapore, 2002.
(23) Chang, B. Y.; Solá, I. R.; Malinovsky, V. S.; Santamaría, J. *J. Chem. Phys.* **2000**, *113*, 4901.
(24) Schinke, R. *Photodissociation Dynamics*; Cambridge University Press: Cambridge, U.K., 1993.
(25) We may notice that if the separation of the equilibrium configurations from X to B and B to C were similar, and if the intermediate potential would be approximately symmetric (for instance, harmonic), then the mapping of the wave functions of X and B in A would be identical, that is, the curves in Figure 2a would overlap. It can be argued that this situation provides more stability to the STIRAP scheme, since for the maximum Franck−Condon amplitude going from and leading to $v = 0$, $p_{0,m}^{X,A} = p_{m,0}^{A,B}$, corresponds a zero Franck−Condon in the adjacent transition going from and leading to $v = 1$.
(26) Malinovsky, V. S.; Solá, I. R. Unpublished results.
(27) The theoretical estimation of the adiabatic threshold requires evaluating the nondiagonal terms of the kinetic coupling, $\mathscr{R}_a^{-1}(x,t)\mathscr{T}\mathscr{R}_a(x,t)$, between the $\Phi_0(x,t)$ and $\Phi_\pm(x,t)$, and of the time-dependent coupling, $\mathscr{R}_a^{-1}(x,t)(\partial/\partial t)\mathscr{R}_a(x,t)$, between the same states, and compare these values with the energy difference between the adiabatic potentials, $|U_\pm^{LIP}(x,t) - U_0^{LIP}(x,t)|$. Averaged quantities can be obtained by integrating over space and time, particularly along the trajectory of the wave packet $\Phi_0(x,t)$. In practice these terms may be evaluated in a different representation.
(28) This, of course, is consistent with the fact that $U_0^{QAP}(x,t) = U_1(x) \cos^2 \theta(t) + U_3(x) \sin^2 \theta(t) \approx U_1(x)$, and therefore, the potential that experiences the initial wave function in the quasi-adiabatic representation is equivalent to the potential that experiences the initial wave function in the diabatic representation.